

Changing-look active galactic nuclei: close binaries of supermassive black holes in action

Jian-Min Wang^{1,2,3} and Edi Bon⁴

¹ Key Laboratory for Particle Astrophysics, Institute of High Energy Physics, Chinese Academy of Sciences, 19B Yuquan Road, Beijing 100049, China, e-mail: wangjm@ihep.ac.cn

² School of Astronomy and Space Sciences, University of Chinese Academy of Sciences, 19A Yuquan Road, Beijing 100049, China

³ National Astronomical Observatories of China, Chinese Academy of Sciences, 20A Datun Road, Beijing 100020, China

⁴ Astronomical Observatory Belgrade, Volgina 7, 11060 Belgrade, Serbia

ABSTRACT

Changing-look active galactic nuclei (CL-AGNs) as a new sub-population are challenging some fundamental physics of AGNs since timescales of the phenomenon hardly reconcile with accretion disk models. In this *Letter*, we demonstrate the extreme case that close binaries of supermassive black holes (CB-SMBHs) with high eccentricities are able to trigger the CL transition through one orbit. In this scenario, binary black holes build up their own mini-disks via peeling gas off inner edges of the circumbinary disk during the apastron phase after then they tidally interact with the disks during the periastron phase to efficiently exchange angular momentum (AM) within one orbital period. For mini-disks with rotation retrograde to the orbit, the tidal torque rapidly squeezes the tidal parts of the mini-disks into much smaller radius, resulting in an elevated accretion rapidly and short flares before declining into type-2 AGNs. In case of prograde mini-disks, they gain AM from the binary and rotate outward, giving rise to a rapid turn-off from type-1 to -2. Turn-on happens around the apastron phase. CB-SMBHs control cycle transitions between type-1 and -2 with orbital periods but allow diverse properties of light curves of CL-AGNs.

Key words. active galaxies – accretion disks – binary black holes

1. Introduction

Seyfert galaxies are usually classified into two sub-populations known as type-1 and -2 corresponding to with and without broad emission lines, respectively, which have been successfully unified by obscurations of a dusty torus differently orientated to observers (Antonucci 1993; Netzer 2015). Despite of its success, there were five outliers before 1980s, such as, NGC 3516 (Andrillat 1968), NGC 7603 (Tohline & Osterbrock 1976), Fairall 9 (Kollatschny & Fricke 1985), NGC 4151 and 3C 390.3 (Penston & Perez 1984), and Mrk 1080 (Cohen et al. 1986), that undergo type transition from type-1 to -2 on a timescale of \lesssim years, or vice versa but on different timescales. Nowadays, they are known as CL-AGNs, which are a fast increasing population discovered from time domain surveys (e.g. MacLeod et al. 2016; Yang et al. 2018; MacLeod et al. 2019; Graham et al. 2020; Wang et al. 2019), even a new class of changing-look LINERs (Frederick et al. 2019), but also Mg II (Guo et al. 2019) and C IV (Ross et al. 2019) lines. Continuum changes from a few factor to several tens when a type transition happens. Typical Eddington ratios are $\lambda_{\text{Edd}} \approx 0.1$ among CL-quasars at type 1 state (MacLeod et al. 2019). Moreover, CL cannot be explained by obscuration variations according to polarization observations (Hutsemékers et al. 2019; Marin et al. 2019), greatly enhancing it as a puzzle.

Several hypotheses have been suggested for CL-AGNs. Inspired by changes of accretion states of X-ray binaries, Noda & Done (2018) show that evaporation of the inner part of the disk is driving a change of accretion states into a drop giving rise to changing-look of Mrk 1018. This seems to be supported on the analogy of CL-AGNs to X-ray binaries (Ruan et al. 2019; Ai et al. 2020; Liu et al. 2019), but what is the mechanism to

quench the accretion? Cooling fronts driven by a sudden change of magnetic torque at the innermost stable circular orbit lead to changing-state (Ross et al. 2018), or magnetic fields support a geometrically thick disk resulting in magnetically elevated accretion onto SMBHs (Dexter & Begelman 2019), or radiation pressure instability (Sniegowska et al. 2020). With the standard model of a single SMBH system for AGNs (Rees 1984), we hardly reconcile the shorter timescales of CL properties to various instabilities of accretion disks since the later is much longer (Ross et al. 2018; Lawrence 2018), even with a few months of CL-AGNs in 1ES 1927+654 (Trakhtenbrot et al. 2019). These facts strongly imply a necessity of external torque for the fast type transition of AGNs. Considering that CL-AGN spectra are characterized by highly asymmetric profiles of broad emission lines, one of the most natural sources driving fast transitions is the secondary black hole in galactic centers.

In this Letter, we show one possibility that CB-SMBHs with high eccentric orbits can trigger type transitions. In such a context, the tidal torque of black holes acting on the mini-disks can efficiently exchange angular momentum (AM) with the binary orbit, giving rise to fast and violent variations of ionizing sources, and consequently AGNs change their appearance.

2. Accretion onto binary black holes

2.1. Close-binaries of SMBHs

Numerous studies on accretion have been done for CB-SMBHs stemming from Artymowicz & Lubow (1996) and Armitage & Natarajan (2002). Basic conclusions are: 1) the circumbinary disk (CBD) surrounding the CB-SMBHs has a central cavity

with a radius of $R_{\text{CBD}} \approx 2a(1 + e)$, which is formed by tidal torque of the binary with half-major axis (a) and eccentricity (e); 2) each black hole is efficiently peeling streams of gas off the inner edge of the CBD that rapidly traverse the cavity (MacFadyen & Milosavljević 2008; Roedig & Sesana 2014; Farris et al. 2015a,b; Shi & Krolik 2015; Bowen et al. 2018); 3) the peeled streams form two mini-disks around each members of the binary (Roedig & Sesana 2014; Farris et al. 2014, 2015a,b; D’Orazio et al. 2016; Tang et al. 2018; d’Ascoli et al. 2018; Moody et al. 2019; Bowen et al. 2018, 2019; Muñoz et al. 2020).

We consider one CB-SMBH system, whose separation with phases is described by $D = a(1 - e^2)/(1 + e \cos \theta)$ and θ is the orbital phase angles. The periastron and the apastron are given by $D_{\text{min,max}} = a(1 \mp e)$, respectively, where tidal interaction gets maximally and minimally. CB-SMBH periods are

$$P_{\text{orb}} = \begin{cases} 19.5 a_{3.4k}^{3/2} M_8(1 + q)^{-1/2} \text{ yr}, \\ 3.1 a_{1k}^{3/2} M_8(1 + q)^{-1/2} \text{ yr}, \end{cases} \quad (1)$$

where $a_{1k,3.4k} = a/(1, 3.4) \times 10^3 R_g$ chosen for two kinds of eccentricities to make a turn-off (for a few years of viscosity time for the innermost part of the disks, see Eq.7 and 4, and also for high- e orbits), $R_g = GM_{\bullet}^p/c^2 = 1.5 \times 10^{13} M_8 \text{ cm}$ is the gravity radius, $M_8 = M_{\bullet}^p/10^8 M_{\odot}$ is the primary black hole mass, $q = M_{\bullet}^s/M_{\bullet}^p$ is the mass ratio, G is the gravitational constant and c is the speed of light. H β -BLR radius follows $R_{\text{H}\beta}/R_g \approx 6.4 \times 10^3 (\eta_{0.1}/\kappa_{10})^{1/2} (\dot{M}_{\bullet}/M_8)^{-1/2}$ (Bentz et al. 2013; Du & Wang 2019), indicating that the BLR is located in the CBD, where $\eta_{0.1} = \eta/0.1$ is radiation efficiency and $\kappa_{10} = \kappa_{\text{bol}}/10$ is the bolometric correction factor, $\dot{M}_{\bullet} = \dot{M}_{\bullet} c^2/L_{\text{Edd}}$ is the dimensionless accretion rates (\dot{M}_{\bullet}) and L_{Edd} is the Eddington luminosity. As the last stage prior to merge, CB-SMBHs share one BLR illuminated by both yielding various profiles of broad lines (e.g. Shen & Loeb 2010; Popović 2012).

2.2. Building-up of mini-disks

As characterized configurations, we give four simplest co-planed cases of mini-disks and orbital AM of CB-SMBHs in Fig. 1, whose complexity arises from random accretion of peeled gas and supply onto the SMBHs. There are solid reasons for fully chaotic and random accretion onto CB-SMBHs making both prograde and retrograde accretions possible in the context of merged galaxies (Nixon et al. 2011, 2013; Dunhill et al. 2014, see also for details in Roedig et al. 2012; Roedig & Sesana 2014 and hereafter). Observationally, there is increasing evidence for random accretion such as SINFONI observations showing two tongues from south and north in $\sim 10 \text{ pc}$ regions in NGC 1068 (Müller Sánchez et al. 2009), dual AGNs with anti-parallel AM in Arp 220 (Wheeler et al. 2020) and other (Tremblay et al. 2016; Temi et al. 2018). The inner edge of the CBD significantly differs from the accretion disk around a single black hole: 1) part of lumps (from the $m = 1$ mode) is granted AM from the binary and flung into the inner edge; but 2) turbulences of the CBD disk transfer AM outward driving lumps move inward. Moreover, the peeled gas has very low AM on average, but the AM direction of individual clumps could be random in some degree.

Following Roedig et al. (2014), we assume that the peeling accretion rates of the primary and secondary black holes are $\dot{M}_p = f_p \dot{M}_{\bullet}$ and $\dot{M}_s = f_s \dot{M}_{\bullet}$, respectively, but $f_p + f_s \lesssim 1$, where \dot{M}_{\bullet} is accretion rates of the CBD, f_p and f_s are fractions depending on orbits of CB-SMBHs. For simplicity, we take them as free parameters in this paper. We roughly divide the orbit into

two parts: 1) the apastron phase ($f_i P_{\text{orb}}; f_i \approx 1$) and 2) the periastron phase of $t_{\text{peri}} \approx (1 - e)^{3/2} P_{\text{orb}} \lesssim 0.03 P_{\text{orb}}$ for $e \gtrsim 0.9$, respectively. The mini-disk is accumulating to have a mass of $\Delta M_p = f_i P_{\text{orb}} f_p \dot{M}_{\bullet}$ during the apastron phase (tidal is weak), but the disk is strongly interacting with individual black holes during periastron phase (the peeling is negligible). It has been shown that the peeling rates are significantly modulated by eccentric orbits (Bogdanović et al. 2008), but only the total peeled mass is important to explore whether CB-SMBHs can make a type transition due to tidal interaction.

The peeled gas will form mini-disks around each individual black hole. During one apastron phase, the peeled gas is

$$\frac{\Delta M_{\text{peel}}}{M_{\odot}} = \begin{cases} 4.4 M_8 f_p \dot{M}_{\bullet} f_i P_{20}, \\ 0.4 q_{0.1} M_8 f_s \dot{M}_{\bullet} f_i P_{20}, \end{cases} \quad (2)$$

for the primary and the secondary, respectively, where $q_{0.1} = q/0.1$ and $P_{20} = P_{\text{orb}}/20 \text{ yrs}$. In the inner edge, cooling timescale of the peeled gas is of $t_{\text{cool}} \approx 5.6 T_4^{1/2} n_{10}^{-1}$ hours, where $T_4 = T/10^4 \text{ K}$ and $n_{10} = n/10^{10} \text{ cm}^{-3}$ is the density. We find t_{cool} is much shorter than the free-fall of $t_{\text{ff}} \approx 4.0 r_{4k}^{3/2} M_8 \text{ yrs} \lesssim P_{\text{orb}}$, where $r_{4k} = R/4 \times 10^3 R_g$. Neglecting the complicated processes, we assume the mini-disks to be described by the inner region of the standard model (Shakura & Sunyaev 1973). Surface density, mid-plane temperature and radial velocity of the disks are

$$\begin{cases} \Sigma = 3.5 \times 10^2 \alpha_{0.1}^{-1} \dot{M}_{\bullet}^{-1} r^{3/2} \text{ g cm}^{-2}, \\ T_c = 1.1 \times 10^6 (\alpha_{0.1} M_8)^{-1/4} r^{-3/8} \text{ K}, \\ v_r = 4.3 \times 10^8 \alpha_{0.1} \dot{M}_{\bullet}^2 r^{-5/2} \text{ cm s}^{-1}, \end{cases} \quad (3)$$

provided $\dot{M}_{\bullet} \geq 10^{-3} (\alpha_{0.1} M_8)^{-1/8}$, and works within outer radius of $1.7 \times 10^2 (\alpha_{0.1} M_8)^{2/21} \dot{M}_{\bullet}^{16/21}$, where $\alpha_{0.1} = \alpha/0.1$ is the viscosity. The viscosity timescale (or radial motion one) is

$$t_{\text{vis}} \approx 3.5 \alpha_{0.1}^{-1} M_8 \dot{M}_{\bullet}^{-2} r_{10}^{7/2} \text{ yrs}, \quad (4)$$

where $r_{10} = R/10 R_g$, which is sensitive to \dot{M}_{\bullet} and radius. Given $r = r_{\ast} = 10$, we have $t_{\text{vis}} = 3.5 M_8 \text{ yr}$ denoted as t_{vis}^{\ast} for $\alpha = 0.1$ and $\dot{M}_{\bullet} = 1$, agreeing with characterized transition of CL-AGNs. In order to make a changing-look, the external torque suggested has to necessarily remove AM of the $R \gtrsim 10 R_g$ disk.

Integrating the surface density of Eq. (3), we get the mini-disk mass of $\Delta M_{\text{disk}}/M_{\odot} \approx 2.5 \alpha_{0.1}^{-1} \dot{M}_{\bullet}^{-1} M_8^2 r_{20}^{7/2}$, where $r_{20} = R/20 R_g$, yielding outer boundary radii of the primary and the secondary mini-disks from $\Delta M_{\text{disk}} = \Delta M_{\text{peel}}$,

$$\frac{R_{\text{out}}}{R_g} \approx \begin{cases} 23.5 \alpha_{0.1}^{2/7} \dot{M}_{\bullet}^{4/7} M_8^{-2/7} P_{20}^{2/7} f_p^{2/7} f_i^{2/7}, \\ 45.3 \alpha_{0.1}^{2/7} \dot{M}_{\bullet}^{4/7} (q_{0.1} M_8)^{-2/7} P_{20}^{2/7} f_s^{2/7} f_i^{2/7}, \end{cases} \quad (5)$$

respectively. Circularization of the peeled gas relies on its AM, but the present model takes a conservative estimate of low AM (since $R_{\text{out}} \ll R_{\text{CBD}}$). The disks keep a vertical equilibrium with a very short timescale of $t_{\text{eq}} = \Omega_K^{-1} = 0.5 M_8 r_{20}^{3/2} \text{ days}$, which is equal to the free-fall timescale (t_{ff}) after accretion disk AM is removed. With the sound speed of $c_s \approx 10^4 T_c^{1/2} \text{ cm s}^{-1}$, we have the radial dynamical timescale of $t_{\text{dyn}} = 1.6 \alpha_{0.1}^{1/8} M_8^{9/8} r_{20}^{19/16} \text{ yrs}$, indicating that the disk keeps as one global under tidal perturbations. Moreover, viscosity time scales of the entire mini-disks are $t_{\text{vis}} \approx (69.6, 692.5) \alpha_{0.1}^{-1} M_8 \dot{M}_{\bullet}^{-2} \text{ yr}$ at R_{out} given by Eq.(5), respectively, which are much longer than P_{orb} . Peeled gas rates are modulated by orbital motion (e.g., Bogdanović et al. 2008; Miranda et al. 2017) with about P_{orb} , but the modulated rates are smeared by the viscosity so that temporal radiation (light curves) from the mini-disks do not follow the orbital modulations. Thus only the total peeled mass is important for the current issues.

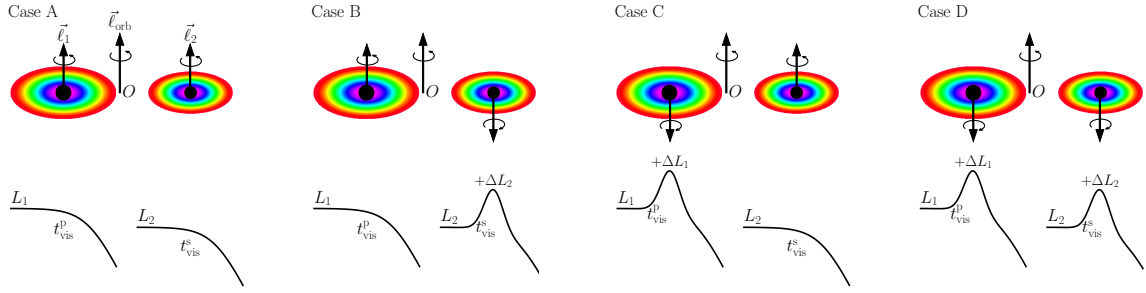


Fig. 1. The simplest configurations of CB-SMBHs and corresponding light curves when the companions pass through the periastron. ($\ell_p, \ell_{\text{orb}}, \ell_s$) denote the AM of the primary, orbital and the secondary black holes, respectively. O is the mass center of the binary. Tidal interaction between mini-disks and SMBHs is leading to two kinds of quenching modes: 1) fast gains of AM for prograde mini-disks (Case A) from the binary orbit; 2) precursor-flaring and quenching for a retrograde mini-disk (the secondary in Case B). The precursor-flaring is caused by the rapid loss of AM of the tidal part so that it greatly enhances accretion of the rest part of the mini-disk. Here $\Delta L_{1,2} = \eta (\delta M_t^{p,s} / r_v^{p,s}) c^2$ represent the increased luminosity (mainly in UV band) due to the elevated accretion for the primary and the secondary BHs, respectively (see text for details).

2.3. Tidal torque from individual black hole

Resultant effects of tidal torques acting on mini-disks depend on the above configurations. For a prograde mini-disk (ℓ_i is parallel to $\ell_{\text{orb}}, i = 1, 2$), the tidal torque will physically divide the mini-disk into two parts at radius R_{tid} (in Eq. 7). In such a case, the inner part of the mini-disks ($\leq R_{\text{tid}}$) is tidal free whereas its tidal part is being accelerated through delivering orbital AM to the part and becomes a “decretion disk”, leading to dramatical decrease of accretion rates with $t_{\text{vis}}^{\text{p}}$ and quench accretion. On the contrary, for a retrograde mini-disk, its the tidal part efficiently losses AM and is rapidly squeezed into tidal radius ($\sim t_{\text{ff}}$), dramatically elevating the ongoing accretion rates making a flare until the inner part diminishes. The tidal interaction between the black holes and the mini-disks results in diverse phenomena of CL-AGNs.

The tidal force acting on the secondary disk by the primary black hole is $F_{\text{tid}} \approx \pm G M_p^2 \delta M_{\text{tid}} D^{-2} (R_d/D)$, where δM_{tid} is the mass of the tidal part at radius R_d . This net tidal force depends on AM configurations in Fig. 1. Here “ \pm ” represents gain and loss of AM from tidal interaction for prograde and retrograde mini-disks, respectively. The tidal torque is approximated by

$$\mathcal{T}_{\text{tid}} \approx \pm \delta M_{\text{tid}} c^2 \left(\frac{R_g}{D} \right) \left(\frac{R_d}{D} \right)^2. \quad (6)$$

Considering that the AM of the tidal part is approximated by $\delta \mathcal{L}_d \approx \delta M_{\text{tid}} \ell_d$, where $\ell_d = \sqrt{G M_p R_d}$ is the specific AM, we have the tidal radius from the balance given by $\delta \mathcal{L}_d = \mathcal{T}_{\text{tid}} t_{\text{peri}}$

$$\frac{R_{\text{tid}}}{R_g} = \left(\frac{\xi_q}{4\pi^2} \right)^{1/3} \left(\frac{a\mathcal{E}}{R_g} \right) = \begin{cases} 14.4 \xi_{0.11}^{1/3} a_{3.4k} \mathcal{E}_{0.03}, \\ 14.1 \xi_{0.11}^{1/3} a_{1k} \mathcal{E}_{0.1}, \end{cases} \quad (7)$$

where $\xi_q = q(1+q)$, $\xi_{0.11} = \xi_q/0.11$ for $q = 0.1$, $\mathcal{E} = (1-e)$ and $\mathcal{E}_{0.03,0.1} = \mathcal{E}/(0.03, 0.1)$ for $e = (0.97, 0.9)$, respectively.

Density waves excited by the torque in the tidal part strong enough to form shocks and to transport AM (Spruit 1987). Recent simulations show this is a powerful way of transporting AM outward (Ju et al. 2016), even stronger than the known MRI (Ryan & MacFadyen 2017). With the help of $\delta \mathcal{L}_d$, we have the timescale of exchanging the AM, $t_{\text{tid}} = \delta \mathcal{L}_d / |\mathcal{T}_{\text{tid}}|$, namely

$$t_{\text{tid}} = q^{1/2} \frac{R_g}{c} \left(\frac{D}{R_g} \right)^{3/2} \left(\frac{R_d}{D} \right)^{-3/2}, \quad (8)$$

with wave density pattern velocity V_{sp} . The mini-disks respond to the tidal perturbations with t_{dyn} . The spiral shocks excited

by the tidal torque are non-local with Mach numbers of $\mathcal{M} = V_{\text{sp}}/c_s = t_{\text{dyn}}/t_{\text{tid}}$ beyond a radius at $\mathcal{M} = 1$

$$\frac{R_{\text{sh}}}{R_g} = \begin{cases} 5.9 \alpha_{0.1}^{-2/43} q_{0.1}^{8/43} M_8^{-2/43} a_{3.4k}^{48/43} \mathcal{E}_{0.03}^{48/43}, \\ 5.8 \alpha_{0.1}^{-2/43} q_{0.1}^{8/43} M_8^{-2/43} a_{1k}^{48/43} \mathcal{E}_{0.1}^{48/43}, \end{cases} \quad (9)$$

and the propagation timescale ($t_{\text{sh}} = t_{\text{dyn}} = t_{\text{tid}}$) is

$$t_{\text{sh}} = \begin{cases} 1.2 \alpha_{0.1}^{3/43} q_{0.1}^{-12/43} M_8^{46/43} a_{3.4k}^{57/43} \mathcal{E}_{0.03}^{57/43} \text{ yr}, \\ 1.1 \alpha_{0.1}^{3/43} q_{0.1}^{-12/43} M_8^{46/43} a_{1k}^{57/43} \mathcal{E}_{0.1}^{57/43} \text{ yr}. \end{cases} \quad (10)$$

Here we take $D = D_{\text{min}}$ for the minimum timescale. We find that $t_{\text{sh}} < t_{\text{vis}}$ indicating that spiral shocks can efficiently exchange the AM of the mini-disk with the binary. Moreover, the condition of $t_{\text{vis}} \lesssim P_{\text{orb}}$ is necessary for a turn-off of accretion onto SMBHs. Combining Eqs.(1,4,7), we have

$$\dot{\mathcal{M}} \gtrsim \begin{cases} 0.8 \alpha_{0.1}^{-1/2} \mathcal{E}_{0.03}^{7/4} q_{0.1}^{7/12} (1+q)^{5/6} a_{3.4k}, \\ 1.9 \alpha_{0.1}^{-1/2} \mathcal{E}_{0.1}^{7/4} q_{0.1}^{7/12} (1+q)^{5/6} a_{1k}, \end{cases} \quad (11)$$

implying $\lambda_{\text{Edd}} = \eta \dot{\mathcal{M}} \gtrsim 0.1$, otherwise, the turn-off cannot be done within one orbital period. Considering large uncertainties of M_{\bullet} and bolometric luminosity, Eq.(11) is roughly consistent with those $\lambda_{\text{Edd}} \gtrsim 0.1$ CL-AGNs (see Fig. 6 in MacLeod et al. 2019), showing the validity of the present turn-off mechanism.

For a prograde case, on the other hand, the decretion disk could be changed into elliptical shapes so that some of it will be accreted onto SMBHs, leading to an inefficient turn-off. We keep this effect in mind for numerical simulations in the future.

2.4. Gravitational waves

Owing to gravitation waves (GWs), the binary orbit is shrinking with a timescale given by (see Eq. 5.6 in Peters 1964),

$$t_{\text{GW}} \approx \begin{cases} 1.8 \times 10^4 \xi_{0.11}^{-1} M_8 a_{3.4k}^4 \mathcal{E}_{0.03}^{7/2} \mathcal{I}_{4.2}^{-1} \text{ yrs}, \\ 8.9 \times 10^3 \xi_{0.11}^{-1} M_8 a_{1k}^4 \mathcal{E}_{0.1}^{7/2} \mathcal{I}_{3.7}^{-1} \text{ yrs}, \end{cases} \quad (12)$$

corresponding to $N_{\text{orb}} \approx (908, 2881)$ orbits, respectively, where $\mathcal{I}_e = 1 + 73e^2/24 + 37e^4/96$, and $\mathcal{I}_{4.2,3.7} = \mathcal{I}_e/(4.2, 3.7)$ for e previously given. The intrinsic strain amplitude is

$$h_s = 7.0 \times 10^{-18} q_{0.1} (1+q)^{-1/3} M_8^{5/3} P_{20}^{-2/3} d_{100}^{-1}, \quad (13)$$

from $h_s = (128/5)^{1/2} (G M_c)^{5/3} (\pi f_{\text{GW}})^{2/3} / c^4 d_L$, $f_{\text{GW}} = 2/P_{\text{orb}} \approx 62.0 P_{20}^{-1}$ nHz is the frequency of GWs, $M_c = q^{3/5} M_{\bullet}^{p^{4/5}} (1 +$

$q)^{-1/5}$ is the chirping mass and $d_{100} = d_L/100 \text{ Mpc}$ is the distance (e.g. Graham et al. 2015). For pure GW-driven evolution, $t_e \approx (9.3, 32.7)t_{\text{GW}}$ and the initial $e_0 = (0.97, 0.9)$ will reduce to $(0.94, 0.81)$ by dropping half of a , respectively, where $t_e = (d \ln e / dt)^{-1}$ is evolutionary timescale of eccentricity. However, a monotonic e -gain (for $e \gtrsim 0.6$) with accretion of the secondary black hole in retrograde binary can keep high- e orbits prior to merge (Amaro-Seoane et al. 2016). Though e -evolution is complicated, the high- e orbits can be kept in some orbits resulting in type transitions of AGNs.

In this paper, we only focus on the extreme cases in which CL transition is triggered by one tidal interaction during one orbit. If the initial eccentricities of CB-SMBH orbits are not as high as $e \approx 0.9$, the CB-SMBHs may undergo tidal interaction for several orbits and lead to CL-transition, or undergo increases of e in the case of retrograde accretion and finally leading to a transition. In such a context, the mini-disks can accumulate more during several orbital periods, CL-AGNs have different variations from that discussed here. A future paper will study the intermediate- e cases.

3. Turn-on and turn-off

As shown in Fig. 1, we focus on four simplest configurations: (1) Case-A ($\uparrow, \uparrow, \uparrow$); (2) Case-B ($\uparrow, \downarrow, \uparrow$); (3) Case-C ($\uparrow, \downarrow, \downarrow$) and (4) Case-D ($\downarrow, \downarrow, \uparrow$). In this paper, we neglect spins of black holes, avoiding more configurations. We note that appearance of Case-B and -C could be less than that of Case-A and -D. For convenient discussions, we use $\delta M_t^{p,s}$ as the masses of the tidal parts of the primary and secondary mini-disks, respectively, and $\delta M_0^{p,s}$ as the rest parts. We stress that the discussions are only valid for characterized properties of the process.

3.1. Case A

In Case A, both mini-disks are prograde. Tidal torque transfers orbital AM to both disks simultaneously so that the tidal parts (with mass of $\delta M_t^{p,s}$) become decretion disks rotating outward (e.g., Rafikov 2016), and accretion onto the binary is interrupted after the mass ($\delta M_0^{p,s}$) of the non-tidal part is depleted. We call this the rest accretion, which is radiating at luminosities of $\Delta L_A = \eta(\delta M_0^p/t_{\text{vis}}^p + \delta M_0^s/t_{\text{vis}}^s)c^2$, where $t_{\text{vis}}^{p,s}$ are viscosity timescales of the primary and secondary mini-disks. According to the standard disk model, photons (ϵ) are emitted from $R_\epsilon/R_g \approx 6(\mathcal{M}/M_8)^{1/3}(\epsilon/13.6\text{eV})^{-4/3}$ as the innermost regions of the mini-disks. Expansion of the tidal part can be simply estimated by $\Delta R_d/R_d \approx 2\Delta(\delta \mathcal{L}_d)/\delta \mathcal{L}_d = 2$ since the balance of $\delta \mathcal{L}_d = \mathcal{T}_{\text{tid}}t_{\text{peri}}$. As a consequence, gas supply to the R_ϵ -region is interrupted by the torque, leading to violent variations of both UV and H β line. Turn-off happens then with a transition from type-1 to -2 after the periastron.

Turn-on transition starts from accumulation via peeling gas from the CBD after the periastron phase. First, the tidal part begins to fall back but with a time scale much longer than t_{vis} by a factor of $(\Delta R_d/R_d)^{7/2} \approx 11.3 (> P_{\text{orb}})$. Second, peeled gas continues to accumulate since the rotating-outward gas is still bounded by its black hole in the same disk plane (since $t_{\text{eq}} \ll t_{\text{dyn}}$). This results in continuous growth of the mini-disks from peeled gas over every orbiting cycles until the mini-disk radii exceed the Roche radius given by $R_H \approx 0.27q^{0.3}a$ for the primary and secondary mini-disks, respectively (Bowen et al. 2017). With limitation of GW-driven timescales of orbit decays, on the other hand, the CB-SMBHs will undergo cycles of $n_{\text{cyc}} \approx t_{\text{GW}}/P_{\text{orb}} \sim 10^3$ around the apastron phase for

$P_{\text{orb}} \sim 20 \text{ yr}$ and $t_{\text{GW}} \sim 2 \times 10^4 \text{ yr}$. Mini-disks then grow up to outer radius of $R_{\text{out}}/R_g \approx (88, 170)$ (by multiplying the factor f_t with n_{cyc} in Eq.5) but $R_{\text{out}}/R_g \leq R_H$ for the primary and secondary, respectively. This disk is able to produce optical continuum emissions like normal AGNs. The innermost regions are undergoing violent variations resulting in fast and large variabilities only in UV but relatively less variable in optical. This agrees with the fact that most CL-AGNs show violent UV continuum but optical less variable (Ross et al. 2018; Lawrence 2018).

Growth of prograde mini-disks results from the circularization of the peeled gas through AM composition. Kinetic energy will be dissipated in this process to radiate some energies (but spectral energy distributions depend on the composition). Consequently, this gives rise to complicated variations of continuum with various timescales. More work needs to be done for details through numerical simulations in the future.

3.2. Case B and C

In Case B, the primary mini-disk is prograde to the orbit whereas the secondary is retrograde. The primary disk is getting AM from the orbit and UV emissions are declining as in Case A, but the secondary shows a flare in UV before quenching. This is caused by a fast increase of accretion rates within R_{tid} through a rapidly squeezing of the δM_t^s due to loss of its AM. The enhanced rates of accretion can be roughly estimated by $\dot{M}_s \approx (\delta M_0^s + \delta M_t^s)/t_{\text{vis}}^s$. The elevated accretion leads to increased luminosity $\Delta L_2 = \eta(\delta M_t^s/t_{\text{vis}}^s)c^2$. After a fast accretion within R_{tid} , the mini-disk is quenched, and consequently, turn-off happens with a timescale of $\sim 1 \text{ yr}$ (Eq. 4). Interestingly, such a flare was found as a precursor of CB-SMBHs from numerical simulations in Chang et al. (2010). In such a case, the primary is contributing optical emissions, but both of them contribute to violent variations of UV emissions. In particular, the gas squeezed by tidal torque is undergoing supersonic infall and may lead to emissions of γ -rays in short timescales (Kolykhalov & Syunyaev 1979; Meszaros & Ostriker 1983), detectable by *Fermi*.

Similar to Case B, but the primary mini-disk in Case C is retrograde to the orbit. It will undergo a flare first and then decay. The secondary mini-disk is quenched as in Case A, which is driven to rotate outward, but it is in charge of optical emissions similar to Case B. We note that the flaring and quenching timescales of the two mini-disks could be different depending on black hole masses, accretion rates and the binary orbit.

3.3. Case D

In Case D, both mini-disks are retrograde. Both tidal parts of the disks are squeezed rapidly into $\leq R_{\text{tid}}$ regions, elevating accretion rates of the disks. After then, a turn-off transition happens. In such a case, the total accretion rates of flare luminosity of the binary is about $\dot{M}_{\text{tot}} = \dot{M}_p + \dot{M}_s$, where $\dot{M}_{p,s} = (\delta M_0^{p,s} + \delta M_t^{p,s})/t_{\text{vis}}^{p,s}$. It should be noted that the enhanced accretion depends on black hole mass and thus the two flares of the mini-disks last on different timescales. These characterized light curves depend on the ratios of $\delta M_t^{p,s}/\delta M_0^{p,s}$ and their relative timescales of viscosity. For cases of extreme eccentric orbits, the mini-disks may be completely tidal destroyed if $R_{\text{tid}} \sim 6R_g$ for extreme cases with very high- e orbits. In such a case, the flares will be enhanced as a result of squeezing of the entire mini-disks into black hole.

Real situations of mini-disks or orbits in CB-SMBHs may be more complicated than the present, such as warped and non-coplanar, such as in OJ 287 (Sillanpää et al. 1988). Moreover, the relative appearance of the four cases remains open, but Case-A and -D could be more common than others. Finally, it should be pointed out that the current scenario provides a cycle of changing-look transition with orbit period in the non-periodical light curves of continuum. Turn-on and turn-off timescales are determined by the orbit, but they could be of quasi-periodicity if considering that the CBD is self-gravitating to form clumps.

4. Conclusions and discussions

CL-AGNs show a puzzle about such a rapid change. In light of heuristic information from observations, we demonstrate the extreme case that CB-SMBHs with low mass ratios and high eccentricities would perform a fast transition of states within one orbit in this Letter. Both black holes are peeling gas off the inner edge of the circumbinary disk to form mini-disks around them. In such a system, tidal torque on the mini-disks risen by companion black holes are strong enough to exchange AM between the disks and the binary orbit for rapid changes of disk innermost regions. Fates of the mini-disks are undergoing either being squeezed into the innermost regions or being expanded outward (to form a decretion disk), depending on AM configurations of the binary system. The different configurations give rise to diverse properties of CL-AGNs including flaring precursors of type transitions. CB-SMBHs are driving changing-look of AGNs to appear transition cycles likely with orbital periods (or quasi-periodical transition due to complications of the inner edge of the CBD). This present scenario can be tested by the turn-on and turn-off behaviors from historical data of spectral variations over several decades. CL-AGNs could contribute significant fractions of low-frequency gravitational wave background.

Several aspects should be investigated for nature of CL-AGNs. First, details of their host morphology should be checked for signatures of disrupted or ripples as merged remnants. This is inspired by Charlton et al. (2019) who found clearly such features from *Gemini* images of four CL-quasars. Second, CL-AGNs could be characterized by profile asymmetries of broad emission lines. We have visually checked on broad-line profiles of CL-AGNs and found *all* of them have either highly-asymmetric or double-peaked profiles, but vice versa is not supported by current observations. Monitoring AGNs with H β Asymmetry (MAHA) is a long term campaign searching for CB-SMBHs (Du et al. 2018). We hope see signals of CB-SMBHs from their 2D transfer functions (Wang et al. 2018; Kovačević et al. 2020a; Songsheng et al. 2020, see a recent review of Wang & Li 2020) as well as ones revealed by GRAVITY/VLTI (Songsheng et al. 2019; Kovačević et al. 2020b). CL-AGNs could be the best candidates of CB-SMBHs. Third, spectral energy distributions of CL-AGNs are poorly understood at epochs of type transitions. That CB-SMBHs are driving the much more violent variations in UV than in optical seems support the present scenario, but complicated processes of the tidal interaction may lead to γ -rays from the inflows with low AM. Monitoring campaigns of CL-AGN multi- λ continuum will greatly help understand on-going physics.

We will study temporal details of the tidal interaction and accretion rates of both mini-disks along the binary orbit in future work. This allows us to compare with observed light curves of CL-AGNs, or to predict some precursors of CL transition, and reveal the peeling physics between the binary and the CBD from observations. In such a context, time-dependent accretion

(and decretion) disks should be employed including the spectral energy distributions. Finally, CL-AGNs could significantly contribute to GW background and this will be done in the future.

Acknowledgements. We are grateful to an anonymous referee, and T. Bogdanović for helpful discussions as well as Z. Yu, Y.-R. Li and Y.-Y. Songsheng from the IHEP AGN group. We acknowledge the support by National Key R&D Program of China through grant -2016YFA0400701, by NSFC through grants NSFC-11991050, -11991054, -11833008, -11690024 and by Grant No. QYZDJ-SSW-SLH007 from the Key Research Program of Frontier Sciences, CAS, by the Strategic Priority Research Program of the CAS grant No.XDB23010400.

References

- Ai, Y., Dou, L., Yang, C., et al. 2020, *ApJ*, 890, L29
Amaro-Seoane, P., Maureira-Fredes, C., Dotti, M., et al. 2016, *A&A*, 591, 114
Andrillat, Y. 1968, *AJ*, 73, 862
Antonucci, R. 1993, *ARA&A*, 31, 473
Armitage, P. J. & Natarajan, P. 2002, *ApJ*, 567, L9
Artymowicz, P. & Lubow, S. H. 1996, *ApJ*, 467, L77
Bentz, M. C., Denney, K. D., Grier, C. J., et al. 2013, *ApJ*, 767, 149
Bogdanović, T. S., Britton, D., Sigurdsson, S., et al., 2008, *ApJS*, 174, 455
Bowen, D. B., Campanelli, M., Krolik, J. H., et al. 2017, *ApJ*, 838, 42
Bowen, D. B., Mewes, V., Campanelli, M., et al. 2018, *ApJ*, 853, L17
Bowen, D. B., Mewes, V., Noble, S. C., et al. 2019, *ApJ*, 879, 76
Chang, P., Strubbe, L. E., Menou, K., & Quataert, E. 2010, *MNRAS*, 407, 2007
Charlton, P. J. L., Ruan, J. J., Haggard, D., et al. 2019, *ApJ*, 876, 75
Cohen, R. D., Rudy, R. J., Puetter, R. C., et al. 1986, *ApJ*, 311, 135
d'Ascoli, S., Noble, S. C., Bowen, D. B., et al. 2018, *ApJ*, 865, 140
Dexter, J. & Begelman, M. C. 2019, *MNRAS*, 483, L17
D'Orazio, D. J., Haiman, Z., Duffell, P., et al. 2016, *MNRAS*, 459, 2379
Du, P., Brotherton, M. S., Wang, K., et al. 2018, *ApJ*, 869, 142
Du, P. & Wang, J.-M. 2019, *ApJ*, 886, 42
Dunhill, A. C., Alexander, R. D., Nixon, C. J., et al. 2014, *MNRAS*, 445, 2285
Farris, B. D., Duffell, P., MacFadyen, A. I., et al. 2014, *ApJ*, 783, 134
Farris, B. D., Duffell, P., MacFadyen, A. I., et al. 2015a, *MNRAS*, 447, L80
Farris, B. D., Duffell, P., MacFadyen, A. I., et al. 2015b, *MNRAS*, 446, L36
Frederick, S., Gezari, S., Graham, M. J., et al. 2019, *ApJ*, 883, 31
Graham, M. J., Djorgovski, S. G., Stern, D., et al. 2015, *MNRAS*, 453, 1562
Graham, M. J., Ross, N. P., Stern, D., et al. 2020, *MNRAS*, 491, 4925
Guo, H., Sun, M., Liu, X., et al. 2019, *ApJ*, 883, L44
Hutsemekers, D., Agís González, B., Marín, F., et al. 2019, *A&A*, 625, A54
Ju, W., Stone, J. M., & Zhu, Z. 2016, *ApJ*, 823, 81
Kollatschny, W. & Fricke, K. J. 1985, *A&A*, 146, L11
Kolykhalov, P. I. & Syunyaev, R. A. 1979, *Soviet Ast.*, 23, 189
Kovačević, A. B., Wang, J.-M., & Popović, L. C. 2020a, *A&A*, 635, A1
Kovačević, A. B., Songsheng, Y.-Y., Wang, J.-M., & Popović, L. C. 2020b, *A&A*, arXiv:2010.01317
Lawrence, A. 2018, *Nature Astronomy*, 2, 102
Liu, H., Wu, Q., Lyu, B., & Yan, Z. 2019, arXiv:1912.03972
MacFadyen, A. I. & Milosavljević, M. 2008, *ApJ*, 672, 83
MacLeod, C. L., Green, P. J., Anderson, S. F., et al. 2019, *ApJ*, 874, 8
MacLeod, C. L., Ross, N. P., Lawrence, A., et al. 2016, *MNRAS*, 457, 389
Marín, F., Hutsemekers, D., & Agís González, B. 2019, arXiv:1909.02801
Mészáros, P. & Ostriker, J. P. 1983, *ApJ*, 273, L59
Miranda, R., Muñoz, D. J., & Lai, D., 2017, *MNRAS*, 466, 1170
Moody, M. S. L., Shi, J.-M., & Stone, J. M. 2019, *ApJ*, 875, 66
Muñoz, D. J., Lai, D., Kratter, K., & Mirand, A. R. 2020, *ApJ*, 889, 114
Müller Sánchez, F., Davies, R. I., Genzel, R., et al. 2009, *ApJ*, 691, 749
Netzer, H. 2015, *ARA&A*, 53, 365
Nixon, C., King, A., & Price, D. 2013, *MNRAS*, 434, 1946
Nixon, C. J., Cossins, P. J., King, A. R., et al. 2011, *MNRAS*, 412, 1591
Noda, H. & Done, C. 2018, *MNRAS*, 480, 3898
Penston, M. V. & Perez, E. 1984, *MNRAS*, 211, 33P
Peters, P. C. 1964, *Physical Review*, 136, 1224
Popović, L. C. 2012, *NewAR*, 56, 74
Rahkov, R. R. 2016, *ApJ*, 830, 7
Rees, M. J. 1984, *ARA&A*, 22, 471
Roedig, C., Krolik, J. H., & Miller, M. C. 2014, *ApJ*, 785, 115
Roedig, C. & Sesana, A. 2014, *MNRAS*, 439, 3476
Roedig, C., Sesana, A., Dotti, M., et al. 2012, *A&A*, 545, A127
Ross, N. P., Ford, K. E. S., Graham, M., et al. 2018, *MNRAS*, 480, 4468
Ross, N. P., Graham, M. J., Calderone, G., et al. 2019, arXiv:1912.05310
Ruan, J. J., Anderson, S. F., Eracleous, M., et al. 2019, *ApJ*, 883, 76
Ryan, G. & MacFadyen, A. 2017, *ApJ*, 835, 199
Shakura, N. I. & Sunyaev, R. A. 1973, *A&A*, 500, 33
Shen, Y. & Loeb, A. 2010, *ApJ*, 725, 249
Shi, J.-M. & Krolik, J. H. 2015, *ApJ*, 807, 131
Sillanpää, A., Haarala, S., Valtonen, M. J. et al. 1988, *ApJ*, 325, 628
Sniegowska, M., Czerny, B., Bon, E. & Bon, N. 2020, *A&A*, arXiv:2007.06441
Songsheng, Y.-Y., Wang, J.-M., Li, Y.-R., & Du, P. 2019, *ApJ*, 881, 140
Songsheng, Y.-Y., Xiao, M., Wang, J.-M., & Ho, L. C. 2020, *ApJS*, 247, 3
Spruit, H. C. 1987, *A&A*, 184, 173
Tang, Y., Haiman, Z., & MacFadyen, A. 2018, *MNRAS*, 476, 2249
Tem, P., Amblard, A., Gitti, M., et al. 2018, *ApJ*, 858, 17
Tohline, J. E. & Osterbrock, D. E. 1976, *ApJ*, 210, L117
Trakhtenbrot, B., Arcavi, I., MacLeod, C. L., et al. 2019, *ApJ*, 883, 94
Tremblay, G. R., Oonk, J. B. R., Combes, F., et al. 2016, *Nature*, 534, 218
Wang, J., Xu, D. W., Wang, Y., et al. 2019, *ApJ*, 887, 15
Wang, J.-M., Songsheng, Y.-Y., Li, Y.-R., & Yu, Z. 2018, *ApJ*, 862, 171
Wang, J.-M. & Li, Y.-R. 2020, *RA&A*, 20, 160
Wheeler, J., Glenn, J., Rangwala, N. & Fyhrrie, A. 2020, *ApJ*, 896, 43
Yang, Q., Wu, X.-B., Fan, X., et al. 2018, *ApJ*, 862, 109